Available online at www.sciencedirect.com
ScienceDirect
International Journal of Mass Spectrometry 267 (2007) 30–42
International Journal of Mass Spectrometry
www.elsevier.com/locate/ijms

Cytosine neutral molecules and cation–radicals in the gas-phase Structures, energetics, ion chemistry, and neutralization–reionization mass spectrometry

Jill K. Wolken [a], Chunxiang Yao [a], František Tureček [a,*], Michael J. Polce [b], Chrys Wesdemiotis [b,*]

[a] *Department of Chemistry, Bagley Hall, Box 351700, University of Washington, Seattle, WA 98195-1700, United States*
[b] *Department of Chemistry, University of Akron, Akron, OH, United States*

Received 18 August 2006; received in revised form 2 February 2007; accepted 20 February 2007
Available online 2 March 2007

Abstract

Gas-phase cytosine molecules and cation–radicals represent a complex system of several nearly isoenergetic tautomers within each group. Computational methods differ in ordering the relative enthalpies of neutral cytosine tautomers. At our highest level of theory, CCSD(T)/aug-cc-pVTZ calculations find an enol form, *anti*-2-hydroxy-4-aminopyrimidine (**2**), to be the most stable neutral tautomer in the gas-phase, followed by its rotamer, *syn*-2-hydroxy-4-aminopyrimidine (**3**), the canonical oxo-form, 4-amino-1,2-dihydropyrimidin-2(*1H*)-one (**1**), imino-forms, 2-oxo-4-iminodihydro(*1H*,*3H*)pyrimidine (**4** and **5**), and another oxo-form, 4-amino-dihydropyrimidin-2(*3H*)-one (**6**). Other tautomers, such as *anti-anti*, *syn-syn* and *syn-anti*-2-hydroxy-4-iminodihydro(*3H*,*4H*)pyrimidines (**7**–**9**), are less stable. The adiabatic ionization energies of the major cytosine tautomers have been calculated to be 8.71, 8.64, 8.62, 8.58, 8.64, and 8.31 eV for **1**, **2**, **3**, **4**, **5**, and **6**, respectively. Cytosine cation–radicals show very close relative energies that increase in the order of $\mathbf{6}^{\bullet+}$ (most stable) $<\mathbf{2}^{\bullet+} \approx \mathbf{3}^{\bullet+} < \mathbf{4}^{\bullet+} \approx \mathbf{7}^{\bullet+} \approx \mathbf{1}^{\bullet+} < \mathbf{5}^{\bullet+}$. In addition, distonic ions having radical centers at C-5 ($\mathbf{10}^{\bullet+}$) and C-6 ($\mathbf{11}^{\bullet+}$ are found as low-energy isomers of $\mathbf{1}^{\bullet+}$–$\mathbf{7}^{\bullet+}$. Metastable cytosine cation–radicals undergo ring-cleavage dissociations by eliminations of CO (major) and HN=C=O (minor). The energetics of these and other higher-energy dissociations, including the pertinent transition states, have been established by high-level ab initio and density functional theory calculations and plausible mechanisms have been proposed. Collisional neutralization of cytosine cation–radicals with trimethylamine and dimethyldisulfide as electron donors forms stable molecules that are detected as cation–radicals following collisional reionization. The dissociations observed upon neutralization–reionization mainly include ring-cleavages followed by loss of N=C=O, HN=C=O, and formation of C_2H_3N, C_2H_2N, and CO neutral fragments that are assigned to ion dissociations following reionization.

Keywords: Cytosine tautomers; Cytosine cation–radicals; Ionization energies; Neutralization–reionization; Ab initio calculations

1. Introduction

Ionization of DNA is the primary event that triggers processes contributing to DNA damage via the so-called direct mechanism [1]. The π-electronic systems in the nucleobases are the most likely sites of ionization, and the electron deficiency is presumed to progress along the DNA strand according to the nucleobase ionization energies (IE) that follow the trend IE(thymine) > IE(cytosine) > IE(adenine) > IE(guanine), as established by photoionization measurements [2–6] and theory [7–9]. While bimolecular reactions of nucleobase cation–radicals have been studied extensively by radiolytic methods in solution or solid state [10–14], relatively little is known about unimolecular dissociations of nucleobase cation–radicals in the gas-phase [15–17]. Density functional theory calculations have been reported for the canonical tautomers of nucleobase cation–radicals, and structure changes upon ionization have been discussed [8]. Ionization energies have been reported by both experiment [2–6] and theoretical calculations [7–9], as reviewed recently [18]. There is also a wealth of computational data on the structures and relative stabilities of nucleobase molecules in the gas-phase and clusters

* Corresponding authors. Tel.: +1 206 685 2041; fax: +1 206 685 3478.
E-mail address: turecek@chem.washington.edu (F. Tureček).

1387-3806/$ – see front matter © 2007 Elsevier B.V. All rights reserved.
doi:10.1016/j.ijms.2007.02.016

with water molecules [19]. Cytosine, in particular, has been the subject of detailed computational studies that were motivated by the existence of four tautomers of very similar relative enthalpies that posed a challenge to computational methods. In spite of this wealth of data, there are no studies aimed at the unimolecular reactivity of cytosine cation–radicals and their interactions with electrons. We now report a combined experimental and theoretical study of cytosine molecules and cation–radicals in the gas-phase using high-level ab initio theory and neutralization–reionization mass spectrometry [20–23].

2. Experimental

2.1. Materials

Cytosine (Sigma–Aldrich) was used as received and sampled to the mass spectrometers from heated solid probes. Cytosine-d_3 was prepared by dissolving cytosine (100 mg, 0.9 mmol) in 5 mL D_2O and allowing to stand at 20 °C for 3 days. D_2O was evaporated in vacuo and the solid cytosine-d_3 was used without further purification. A 70 eV electron ionization mass spectrum showed 6% d_1, 29% d_2, 61% d_3 and 4% d_4 species. Collisionally-activated dissociation (CAD) spectra were measured on a JEOL HX-110 double focusing mass spectrometer of EB geometry (electrostatic analyzer E precedes magnetic sector B). Air was admitted to the first field free region at pressures to achieve 70% or 50% transmittance of the precursor ion beam at 10 keV. The CAD spectra were recorded by scanning E and B while maintaining a constant B/E ratio (B/E linked scan). The mass resolution in these linked scans was >500. Metastable ion and CAD spectra (collisions with He) were also obtained as kinetic energy scans on the VG-Autospec tandem mass spectrometer at the University of Akron operating at 8 keV [24]. Neutralization–reionization ($^+NR^+$) mass spectra were measured on the University of Washington (UW) tandem quadrupole acceleration–deceleration mass spectrometer [25]. Cytosine cation–radicals were produced in an electron-impact ion source (200 °C, 1 mA emission current) that was floated at 75–80 V. The ions were transmitted by a wide-open quadrupole mass filter (55–60 V bias) onto an acceleration lens that was floated at −8150 V. A 8225 eV ions were discharged by collisions with dimethyl disulfide that was admitted to the vacuum system at pressures to achieve 70% transmittance of the precursor ion beam. Residual ions were reflected by a special electrostatic lens and the neutral products were allowed to drift to a reionization cell where they were reionized by collisions with molecular oxygen at 70% beam transmittance. The ions were decelerated to 70–75 eV and mass analyzed by a second quadrupole mass analyzer that was floated at 70–75 V and scanned at unit mass resolution. Neutralization–collisional–activation–reionization ($^+NCR^+$) mass spectra were measured by admitting He at 50% beam transmittance into the conduit of the UW instrument, as described previously [26]. Typically, 50–60 scans were collected and averaged to provide the NR and NCR mass spectra presented here. Additional neutralization–reionization mass spectra were measured at 8 keV ion kinetic energy on the VG-Autospec tandem mass spectrometer. Ions were prepared by electron ionization at 200 °C, selected by mass, and neutralized by collisions with trimethylamine at 70% ion beam transmittance. Oxygen was used for reionization at 70% beam transmittance. The spectra were obtained as kinetic energy scans.

2.2. Calculations

Standard ab initio calculations were performed using the Gaussian 03 suite of programs [27]. Optimized geometries were obtained by density functional theory calculations using Becke's hybrid functional (B3LYP) [28–30] and the 6-31+G(d,p) basis set. Another set of structures for several neutral cytosine tautomers were obtained by optimizations that used the Møller–Plesset theory [31] with all-electron excitations (MP2(FULL)) and the 6-31+G(d,p) basis set. Spin unrestricted calculations were performed for all open-shell systems. Stationary points were characterized by harmonic frequency calculations with B3LYP/6-31+G(d,p) as local minima (all real frequencies) and first-order saddle points (one imaginary frequency). The optimized geometries and uncorrected harmonic frequencies are available from the corresponding author (F.T.) upon request. The calculated frequencies were scaled with 0.963 and used to obtain zero-point energy corrections, enthalpies, entropies. The rigid-rotor harmonic oscillator (RRHO) model was used in thermochemical calculations except for low frequency modes where the vibrational enthalpy terms that exceeded $0.5RT$ were replaced by free internal rotation terms equal to $0.5RT$. It has been shown previously [32] that enthalpies and entropies based on the RRHO and free rotation approximations bracket the more accurate values calculated with the hindered internal rotor model, and the small differences cancel out in calculations of relative enthalpies and entropies. Improved energies were obtained by single-point calculations that were carried out at several levels of theory, including split-valence triple-ζ basis sets of increasing size furnished with polarization and diffuse functions, e.g., 6-311G(d,p), 6-311+G(3df,2p), 6-311++G(3df,2p), and 6-311G(3df,2pd), and correlation consistent basis sets cc-pVTZ and aug-cc-pVTZ. The B3LYP and MP2 energies calculated with the large basis set were combined according to the B3-MP2 scheme, as described previously [33,34]. Second, single-point energies were calculated with coupled-cluster theory [35] including single, double, and disconnected triple excitations (CCSD(T)) [36] and the 6-31G(d,p) basis set. These were then extrapolated to effective CCSD(T)/6-311++GG(3df,2p) using the standard formula (Eq. (1))

$$\mathrm{CCSD(T)/6\text{-}311++G(3df,2p)} \cong \mathrm{CCSD(T)/6\text{-}31G(d,p)} + \mathrm{MP2/6\text{-}311++G(3df,2p)} - \mathrm{MP2/6\text{-}31G(d,p)} \quad (1)$$

For selected systems, single-point CCSD(T) calculations were also carried out with Dunning's correlation consistent triple-ζ basis set, cc-pVTZ and aug-cc-pVTZ [37].

RRKM calculations were performed using Hase's program [38] that was recompiled for Windows NT [39]. Unimolecular rate constants were obtained by direct count of quantum states at internal energies that were increased in 2 kJ mol^{-1} steps from the transition state up to 350 kJ mol^{-1} above the reactant.

Rotations were treated adiabatically, and the calculated $k(E, J, K)$ rate constants were Boltzmann-averaged over the thermal distribution of rotational states at 473 K, corresponding to the ion source temperature.

3. Results and discussion

3.1. Cytosine tautomers

Neutral cytosine is known to exist as a mixture of tautomers in the condensed [40,41] and gas-phase [42]. Previous computational studies reported the relative enthalpies and free energies for several tautomeric structures that pointed out the canonical oxo-form, 4-amino-1,2-dihydropyrimidin-2(*1H*)-one (**1**), and the enol tautomers, *anti*-2-hydroxy-4-aminopyrimidine (**2**), and *syn*-2-hydroxy-4-aminopyrimidine (**3**), as the most stable isomers [43–52]. The relevant structures are shown in Fig. 1 which also shows the C, N, and O atom numbering in cytosine. The structures of **1**–**4** that were optimized with B3LYP and MP2(FULL) *show very similar bond lengths and angles*. Some minor differences are observed in the C-2–O bond lengths that are consistently shorter in the B3LYP-optimized structures compared to the MP2(FULL) ones [52]. This indicates that B3LYP calculations favor C–O bonds that have more carbonyl-like character and thus are shorter. Another small difference is in the lengths of the C-4–N_{exo} bonds that are consistently shorter by B3LYP. This may be connected with the generally flatter NH_2 groups in **1**–**3** in B3LYP-optimized structures compared to those from MP2(FULL) [52] as illustrated by the pertinent dihedral angles (Fig. 1). Flattening of the NH_2 group favors π-interaction of the nitrogen lone pair with the ring π-electronic system, resulting in shorter C-4–N_{exo} bonds. These small differences in the optimized structures have very small effects on the calculated relative energies of the cytosine isomers. For example, the relative energies calculated with effective CCSD(T) and comparable basis sets, e.g., 6-311+G(3df,2p) and 6-311++G(3df,2p), show the relative energies of **1**–**4** to be within 1 kJ mol^{-1} between the two sets when based on B3LYP and MP2(FULL) geometries (Table 1).

There has been a consistent discrepancy in the energy ordering of **1** relative to **2** and **3**, as perturbational and coupled-cluster calculations prefer **2** as the most stable structure [49,51], whereas density functional theory calculations, performed with Becke's hybrid B3LYP functional, prefer **1** [45,49]. Our calculations reflect this trend in that MP2 and CCSD(T) calculations with all basis sets we used favored **2** as the most stable isomer, whereas

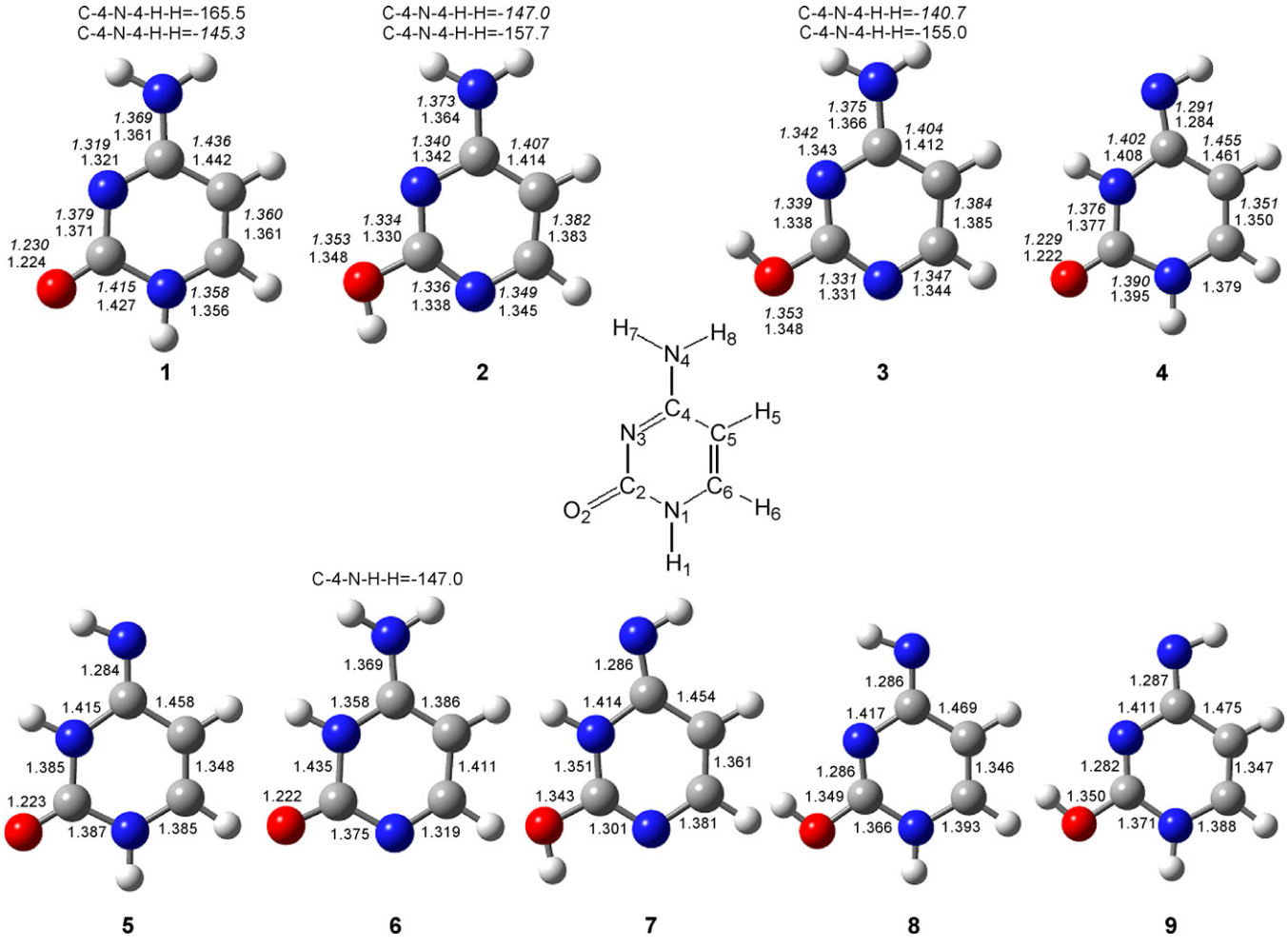

Fig. 1. B3LYP/6-31 + G(d,p) optimized structures of cytosine tautomers **1**–**9**. Bond lengths in angstroms.

Table 1
Relative energies of cytosine tautomers

Method	Tautomer relative energy ($\Delta H^0_{0,g}$)[a]					
	1	**2**	**3**	**4**	**5**	**6**
B3LYP/6-31+G(d,p)	0	2.7	6.0	10.2	17.4	29.0
B3LYP/6-311++G(3df,2p)[b]	0	5.2	8.4	9.9	17.0	29.2
B3LYP/cc-pVTZ[b]	0	4.2	7.3	8.3		
B3LYP/aug-cc-pVTZ[b]	0	4.5	7.6	9.6		
MP2/6-31G(d,p)[b]	0	−6.0	−3.2	4.7	10.9	28.9
MP2/6-311++G(3df,2p)[b]	0	−2.8	0.1	8.5	15.5	31.2
MP2/cc-pVTZ[b]	0	−7.6	−4.7	6.5		
CCSD(T)/6-31G(d,p)[b]	0	−5.4	−2.6	0.6	6.4	28.7
CCSD(T)/6-311++G(3df,2p)[b,c]	0	−2.2	0.7	4.4	11.0	31.0
CCSD(T)/cc-pVTZ[b]	0	−5.6	−2.9	2.7		
MP2(full)/6-31+G(d,p)	0	−4.8	−1.7	9.6		
MP2/6-311G(d,p)[d]	0	−8.8	−5.8	5.1		
MP2/6-311+G(3df,2p)[d]	0	−3.1	−0.1	8.5		
MP2/6-311++G(3df,2pd)[d]	0	−4.7	−1.8	8.0		
MP2/6-311G(3df,2pd)[d]	0	−5.0	−2.1	6.2		
MP2/aug-cc-PVTZ[d]	0	−5.8	−2.9	8.2		
CCSD(T)/6-311G(d,p)[d]	0	−7.3	−4.4	2.0		
CCSD(T)/6-311G(3df,2pd)[c,d]	0	−3.4	−0.7	3.1		
CCSD(T)/6-311+G(3df,2p)[c,d]	0	−1.6	1.3	5.4		
CCSD(T)/6-311++G(3df,2pd)[c,d]	0	−3.2	−0.3	4.9		
CCSD(T)/aug-cc-pVTZ[d]	0	−3.9	−1.1	4.5		
B3-MP2/6-311++G(3df,2p)[e]	0	1.2	4.2	9.2	16.2	30.2
B3-MP2/cc-pVTZ[e]	0	−1.7	1.3	7.4		
B3-MP2/aug-cc-pVTZ[e]	0	−0.6	2.3	8.9		
CCSD(T)/inf + ZPVE[f]	0	−4.9	−2.1	5.3		

[a] In units of kJ mol^{-1} at 0 K and including B3LYP/6-31+G(d,p) zero-point vibrational energy corrections.
[b] Single-point energies on B3LYP/6-31+G(d,p) optimized geometries.
[c] Effective energies from linear basis set extrapolation: E[CCSD(T)/large basis set] ≈ E[CCSD(T)/small basis set] + E[MP2/large basis set] − E[MP2/small basis set].
[d] Single-point energies on MP2(FULL)/6-31+G(d,p) optimized geometries.
[e] E(B3-MP2) = 0.5{E[B3LYP] + E[MP2]}.
[f] From ref. Trygubenko et al. [52].

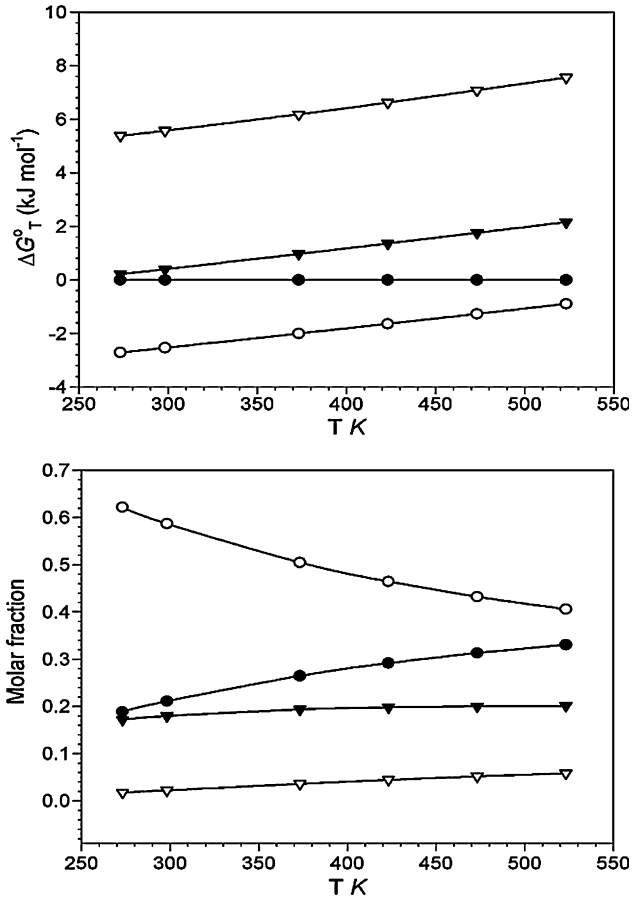

Fig. 2. Relative free energies ($\Delta G^0_{g,T}$, top panel) and equilibrium molar fractions (lower panel) of cytosine tautomers **1**–**4** in the gas-phase as a function of temperature. The relative energies were from CCSD(T)/aug-cc-pVTZ single-point calculations. Full circles: **1**; open circles: **2**; full triangles: **3**; open triangles: **4**.

B3LYP calculations consistently favored **1** (Table 1). The differences are in part cancelled in the B3-MP2 calculations that place **1** very close to **2**, whereby the actual ordering depends on the basis set and tends to prefer **2** in calculations with the largest basis sets (Table 1). In general, the relative energies are sensitive to the type of the basis set used, although convergence is indicated in calculations using the largest basis sets. For example, relative energies calculated with effective CCSD(T) and our largest split-valence basis set, 6-311++G(3df,2pd), are within 0.8 kJ mol^{-1} of those calculated by CCSD(T)/aug-cc-pVTZ. The previous "best" relative energies that were extrapolated from CCSD(T) calculations by Trygubenko et al. [52], are within 1 kJ mol^{-1} of the CCSD(T)/aug-cc-pVTZ values after correction for zero-point energies and presented as $\Delta H^0_{0,g}$ (Table 1).

The relative free energies (ΔG^0_T) for the four most stable tautomers **1**–**4** that are based on the CCSD(T)/aug-cc-pVTZ energies are plotted as a function of temperature in Fig. 2. The ΔG^0_T values determine the equilibrium composition of gas-phase tautomers relevant to ionization and protonation. For example, at the typical ion source temperature of 473 K, a mixture of gaseous cytosine tautomers is calculated to consist of 31% **1**, 43% **2**, 20% **3**, and 5% **4**. By comparison, using another set of relative energies from high-level CCSD(T) calculations of Kobayashi [51] and converting them to ΔG^0_{473} using our ΔH_{473} and ΔS_{473} corrections, we obtain 24% **1**, 47% **2**, 22% **3**, 6% **4**, and 1% **5**, for gas-phase equilibria at 473 K. In spite of some differences in the tautomer relative free energies and equilibrium populations, the high-level calculations agree on the fact that cytosine exists as a mixture of isomers in the gas-phase. The computational mixture analysis is in fair agreement with microwave spectroscopic analysis that indicated the presence of no less than three cytosine tautomers at 295 K [42]. It should be noted that while fast interconversion of rotamers **2** and **3** can occur as a unimolecular process in the gas-phase by OH group rotation (E_{TS} = 35 kJ mol^{-1} relative to **2**), prototropic tautomerizations, e.g., **1** → **2**, **1** → **4**, etc., involve high barriers for unimolecular reactions [53] and are likely to occur as surface-catalyzed reactions [54,55]. The populations of cytosine cation–radicals produced by electron ionization at non-threshold energies (70 eV) are likely to be similar to the populations of neutral cytosine tautomers in the gas-phase at the ion source temperature (473 K). This follows from the pertinent ionization cross sections that are estimated [56] to be very similar for the

Table 2
Cytosine ionization and recombination energies

Tautomer	Ionization	Ionization energy[a]				
		B3LYP/6-31+G(d,p)	B3LYP/6-311++G(3df,2p)	MP2	B3-MP2/6-311++G(3df,2p)	CCSD(T)
1	IE_{adiab}	8.55	8.58	8.84	8.71	8.71
	IE_{vert}		8.68[b]	8.90[b]	8.79[b]	
	RE_{vert}		8.47[c]	8.72[c]	8.60[c]	
2	IE_{adiab}	8.48	8.48	8.76	8.62	8.64
	IE_{vert}		8.69[b]	8.97[b]	8.83[b]	
	RE_{vert}		8.30[c]	8.55[c]	8.42[c]	
3	IE_{adiab}	8.47	8.47	8.76	8.62	8.62
	IE_{vert}		8.71[b]	9.02[b]	8.86[b]	
	RE_{vert}		8.27[c]	8.53[c]	8.40[c]	
4	IE_{adiab}	8.42	8.44	8.67	8.56	8.58
5	IE_{adiab}	8.47	8.50	8.68	8.59	8.64
6	IE_{adiab}	8.22	8.24	8.44	8.34	8.31

[a] Adiabatic ionization energies in units of electronvolt at 0 K including B3LYP/6-31+G(d,p) ZPVE corrections.
[b] Vertical ionization energies.
[c] Vertical recombination energies in cation–radicals.

cytosine tautomers ($13.9 - 14.5 \times 10^{-16}$ cm^2), indicating similar ionization probabilities. The cation–radicals can possibly undergo unimolecular isomerizations that depend on their relative stabilities and the pertinent transition state energies, as discussed below.

3.2. Cytosine ionization energies

The adiabatic ionization energies (IE_a) are similar among cytosine tautomers **1**–**4**, with the calculated values ranging from 8.56 for **4** to 8.71 eV for **1** (Table 2). By comparison, the reported

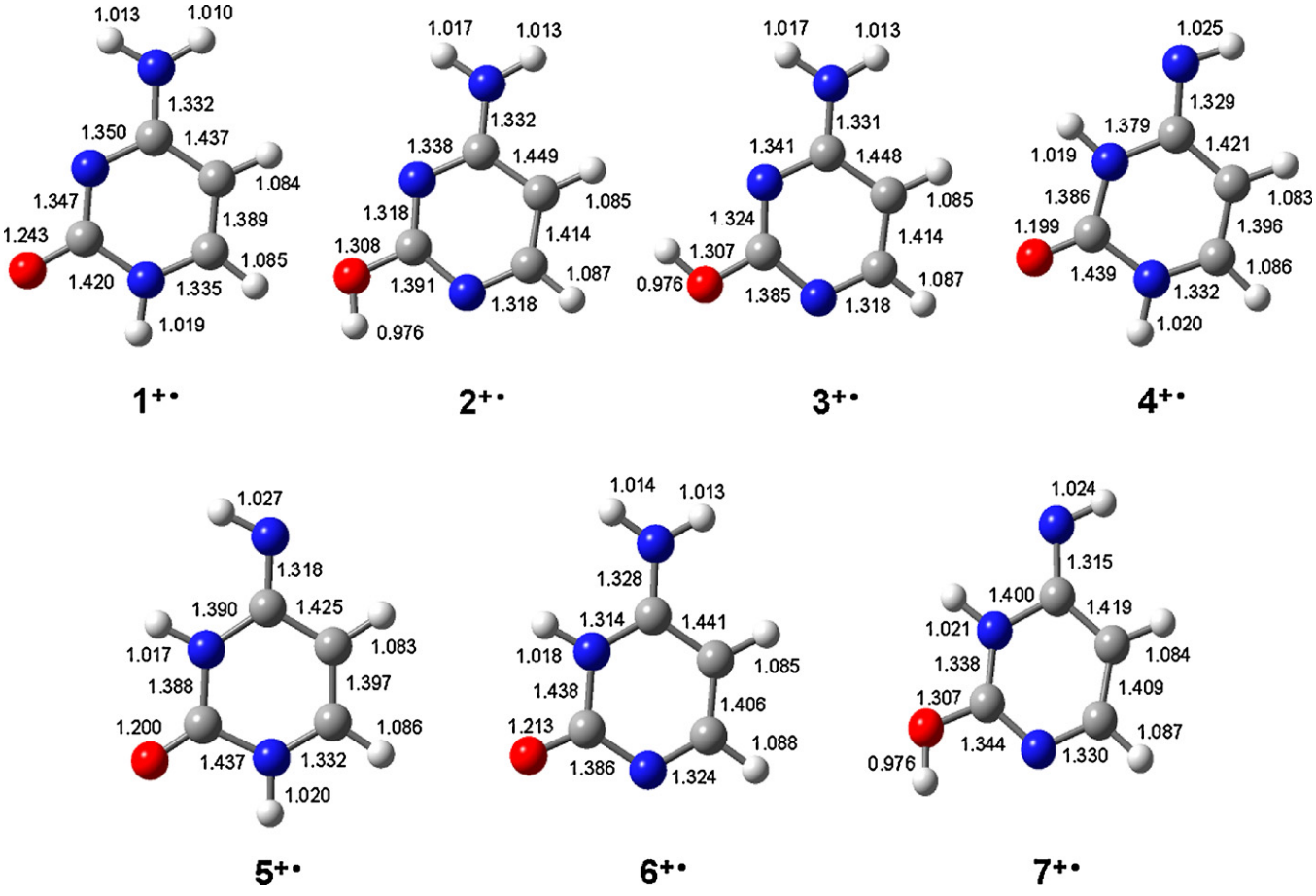

Fig. 3. B3LYP/6-31+G(d,p) optimized structures of cytosine cation–radicals $\mathbf{1}^{\bullet+}$–$\mathbf{7}^{\bullet+}$. Bond lengths in angstroms.

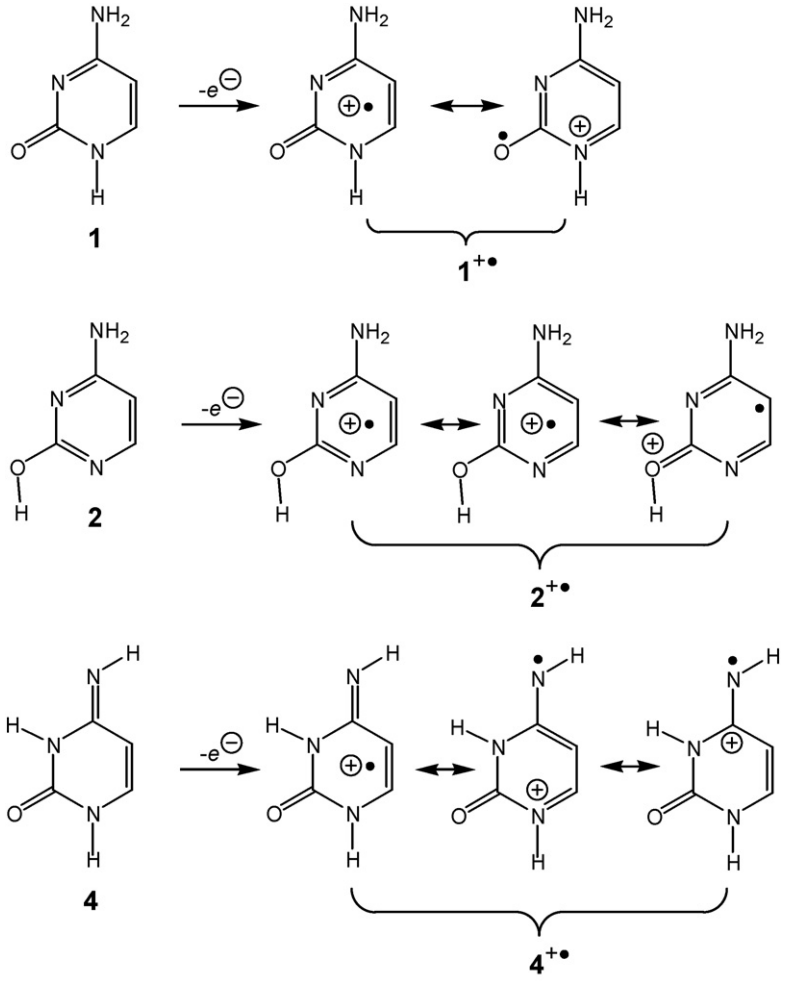

Scheme 1.

experimental ionization energies ranged from 8.45 to 8.9 eV [57], in reasonable agreement with our calculations. Vertical ionization energies (IE_v) of **1**, **2**, and **3** were also calculated and found to be somewhat higher than the adiabatic values, e.g., IE_v = 8.79, 8.83, and 8.86 eV for **1**, **2**, and **3**, respectively. The 0.08–0.24 eV (8–23 kJ mol^{-1}) differences between the adiabatic and vertical ionization energies indicate only moderate excitation in cation–radicals $\mathbf{1}^{\bullet+}$–$\mathbf{4}^{\bullet+}$ upon vertical ionization by electron-impact. The experimental IE_v = 8.94 eV [57], that was measured for a mixture of gas-phase cytosine tautomers, is in acceptable agreement with our calculations. We note that Improta et al. have recently reported their density functional theory calculations of the IE_a and IE_v of cytosine with smaller basis sets that are in general agreement with our results [8].

3.3. Cytosine cation–radical structures and relative stabilities

Cytosine cations–radicals are the main topic of interest in this study. Several local energy minima were found by gradient optimizations for cytosine cation–radicals, as depicted in Fig. 3. The optimized geometries of the cation–radicals show some conspicuous differences from those of the corresponding neutral cytosine tautomers. For example, comparison of the optimized structures of **1** (Fig. 1) and $\mathbf{1}^{\bullet+}$ (Fig. 3) shows that they differ in that the alternating O-2–C-2, N-3–C-4, and C-5–C-6 bonds are longer in the cation–radical while the C-4–N-4 and C-6–N-1 bonds are longer in the neutral molecule. Similar effects on ionization are found for $\mathbf{2}/\mathbf{2}^{\bullet+}$ and $\mathbf{3}/\mathbf{3}^{\bullet+}$ (Figs. 1 and 3). As pointed out by Improta et al. [8] these changes on ionization can be visualized by considering contributions of valence-bond canonical structures for the cation–radicals that result in modified bond orders, as shown in Scheme 1.

The relative energies of cytosine cation–radicals show $\mathbf{6}^{\bullet+}$ as the most stable isomer followed by $\mathbf{2}^{\bullet+}$, $\mathbf{3}^{\bullet+}$, $\mathbf{4}^{\bullet+}$, $\mathbf{7}^{\bullet+}$, and $\mathbf{1}^{\bullet+}$ (Table 3). The energy differences among these tautomeric cation–radicals are very small, indeed, smaller than those found for the neutral cytosine tautomers. An interesting feature is the relative stabilization of ion $\mathbf{6}^{\bullet+}$, which represents the most stable isomer among those studied here, contrasting the ranking of **6** as the sixth most stable among neutral tautomers (Table 1). Cyclic distonic ions $\mathbf{10}^{\bullet+}$ and $\mathbf{11}^{\bullet+}$ that are derived from N-3-protonated **1** by loss of H-5 and H-6, respectively, were also found to be local energy minima (Fig. 4). Although these cation–radicals are less stable than the classical cytosine tautomers, the energy differences are relatively small (Table 3), so that $\mathbf{10}^{\bullet+}$ and $\mathbf{11}^{\bullet+}$

Table 3
Relative and dissociation energies of cytosine cation–radicals

Species/reaction	Relative energy[a,b]		
	B3LYP/6-31+G(d,p)	B3-PMP2[c]/6-311++G(3df,2p)	CCSD(T)[c,d]
1$^{\bullet+}$	0	0	0
1$^{\bullet+}$ → **TS1**	137	129	134
2$^{\bullet+}$	−3	−7	−9
2$^{\bullet+}$ → **TS1**	140	136	144
2$^{\bullet+}$ → **TS2**	161	154	161
3$^{\bullet+}$	−2	−4	−8
3$^{\bullet+}$ → **TS3**	152	150	155
4$^{\bullet+}$	6	−0.3	−1
5$^{\bullet+}$	10	5	4
6$^{\bullet+}$	−4	−7	−11
7$^{\bullet+}$	9	1	−0.1
10$^{\bullet+}$	39	28	27
11$^{\bullet+}$	19	7	7
1$^{\bullet+}$ → **12**$^{\bullet+}$	38	26	33
1$^{\bullet+}$ → **TS4**	39	30	36
1$^{\bullet+}$ → **13**$^{\bullet+}$	67	56	67
1$^{\bullet+}$ → **TS5**	162	158	169
1$^{\bullet+}$ → **14**$^{\bullet+}$	106	90	92
1$^{\bullet+}$ → [3-aminopyrrazole]$^{\bullet+}$ (**15**$^{\bullet+}$) + CO	67	54	39
1$^{\bullet+}$ → **TS6**	160	148	143
1$^{\bullet+}$ → [1,3-diiminopropene]$^{\bullet+}$ (**16**$^{\bullet+}$) + HN=C=O	191	167	179
1$^{\bullet+}$ → **TS7**	251	235	223
1$^{\bullet+}$ → **17**$^{\bullet+}$	88	82	89
1$^{\bullet+}$ → [2-amino-1-azacyclobutadiene]$^{\bullet+}$ (**18**$^{\bullet+}$) + HN=C=O	209	194	198
1$^{\bullet+}$ → [1,5-diazapenta-1,2,4-trienyl]$^{+}$ (**19**$^{+}$) + $^{\bullet}$N=C=O	325	331	317
1$^{\bullet+}$ → [2-amino-1-azacyclobutenyl]$^{+}$ (**20**$^{+}$) + $^{\bullet}$N=C=O	297	294	281
1$^{\bullet+}$ → [pyrimidi-2-one-4-yl]$^{+}$ (**21**$^{+}$) + $NH_2^{\bullet}$	368	345	341
2$^{\bullet+}$ → [2-hydroxypyrimid-4-yl]$^{+}$ (**22**$^{+}$) + $NH_2^{\bullet}$	392	379	373
2$^{\bullet+}$ → [2-hydroxyimidazol-2-yl]$^{+}$ + HC=NH$^{\bullet}$	419	416	392
2$^{\bullet+}$ → [2-hydroxyimidazol-2-yl]$^{+}$ + CH_2=N$^{\bullet}$	381	387	359
1$^{\bullet+}$ → [4-aminoazet-2-one]$^{+}$ (**25**$^{+}$) + CH_2=N$^{\bullet}$	447	440	426
1$^{\bullet+}$ → [oxazol-2-yl]$^{+}$ (**26**$^{+}$) + CH_2=N$^{\bullet}$	407	420	392

[a] In units of kJ mol^{-1} at 0 K including B3LYP/6-31+G(d,p) zero-point vibrational energy corrections.
[b] Relative to **1**$^{+\bullet}$ unless specified otherwise.
[c] From single-point calculations using spin-projected PMP2 energies.
[d] Effective energies from linear basis set extrapolation: E[CCSD(T)/large basis set] ≈ E[CCSD(T)/small basis set] + E[MP2/large basis set] − E[MP2/small basis set].

can occur as intermediates of ion dissociations, as discussed next.

3.4. Cation–radical dissociations

Because of the existence of the tautomer mixture consisting of **1**$^{\bullet+}$, **2**$^{\bullet+}$, **3**$^{\bullet+}$, and **4**$^{\bullet+}$ (vide supra), the mass spectrometric data are generically referred to [cytosine]$^{\bullet+}$ without specifying the tautomer. Elimination of CO is the dominant dissociation of metastable [cytosine]$^{\bullet+}$ (Fig. 5a). The loss of CO from [cytosine]$^{\bullet+}$ shows a dished metastable peak of a large kinetic-energy release, $T_{0.5}$ = 0.550 eV (Fig. 5a, inset). The minor peak for the loss of HN=C=O from metastable [cytosine]$^{\bullet+}$ gives $T_{0.5}$ = 0.030 eV. The metastable-ion dissociations represent the lowest-energy pathways in all tautomers **1**$^{\bullet+}$, **2**$^{\bullet+}$, **3**$^{\bullet+}$, and **4**$^{\bullet+}$, as discussed below. Collisional activation of stable [cytosine]$^{\bullet+}$ produces the CAD mass spectra shown in Figs. 5b and 6a. The CAD mass spectra are quite analogous to the standard 70 eV mass spectrum of neutral cytosine, shown as inset in Fig. 6, and contain fragment ions due to loss of CO (*m/z* 83), NCO (*m/z* 69), HNCO (*m/z* 68), and their complementary ions at *m/z* 43, 42, and 28. The CAD mass spectrum of cytosine-d_3 (Fig. 6b) reveals additional fragmentations that overlapped by mass in Fig. 6a. For example, the presence of an *m/z* 85 fragment indicates loss of a [CHDN]$^{\bullet}$ radical from cytosine-d_3 and [CH_2N] from cytosine; the latter neutral fragment was isobaric with the CO in Fig. 6a. Deuterium labeling also shows possible elimination of H_2N–CN (isobaric with O=C=N$^{\bullet}$) at *m/z* 70 and eliminations of both HN=C=O (*m/z* 71) and DN=C=O (*m/z* 70) in a 2:3.3 ratio, indicating that H/D scrambling occurred in the dissociating ions.

The dissociation mechanisms and energetics for the formation of the major fragment ions were elucidated by ab initio and density functional theory mapping of the pertinent parts of the potential energy surface of the ground doublet states of **1**$^{\bullet+}$–**4**$^{\bullet+}$. The dissociation and transition state energies are summarized in Table 3, the optimized structures of selected intermediates and transition states are given in Figs. 4 and 7.

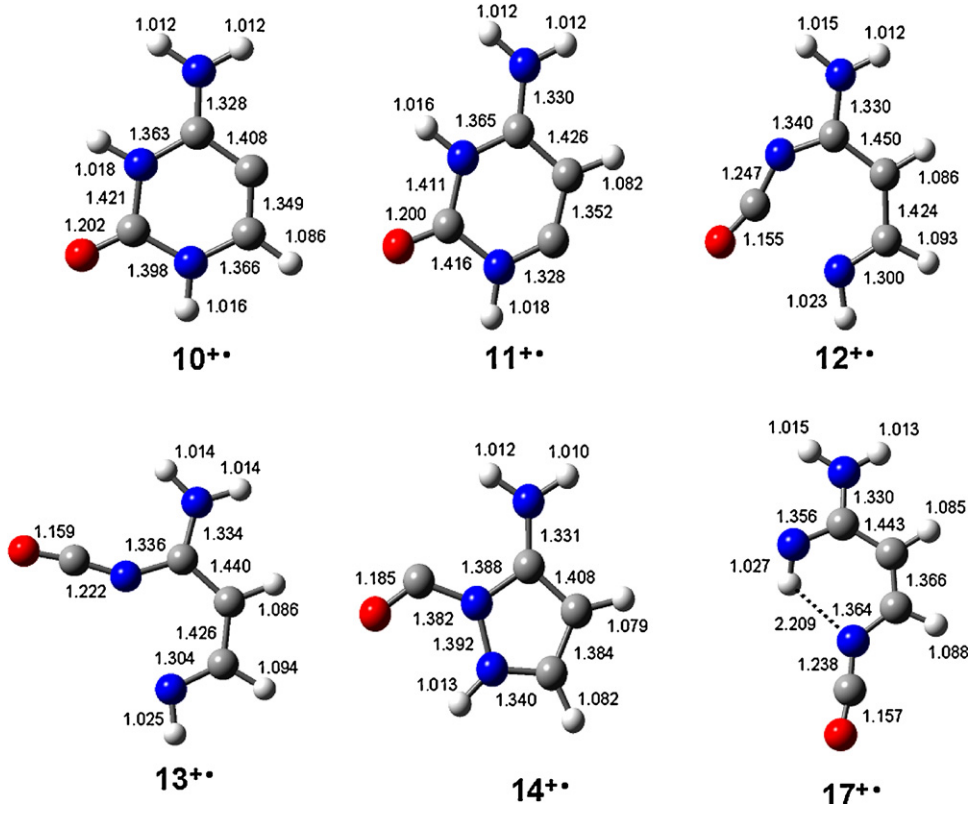

Fig. 4. B3LYP/6-31+G(d,p) optimized structures of dissociation intermediates. Bond lengths in angstroms.

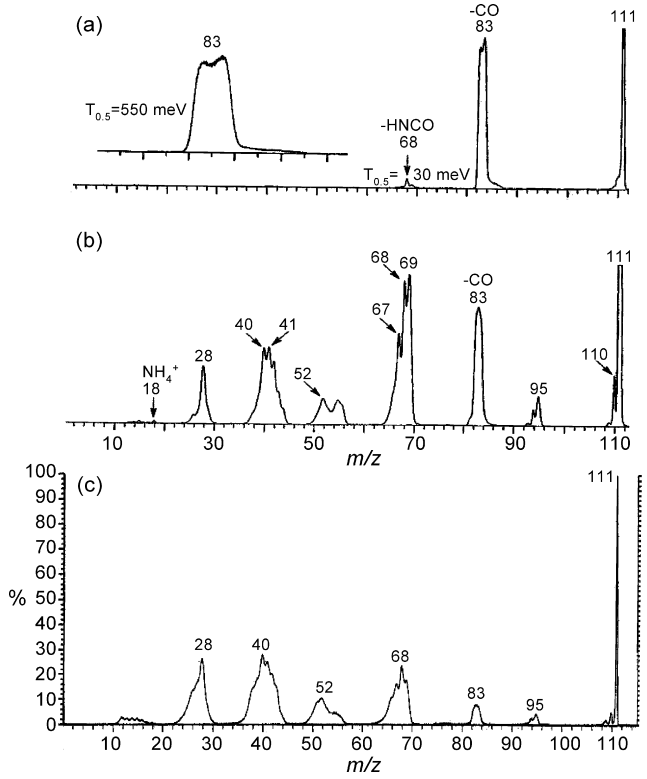

Fig. 5. Tandem mass spectra of [cytosine]•+ obtained as kinetic energy scans. (a) Metastable-ion spectrum. (b) Collisionally-activated dissociation (He) mass spectrum. (c) Neutralization–reionization mass spectrum.

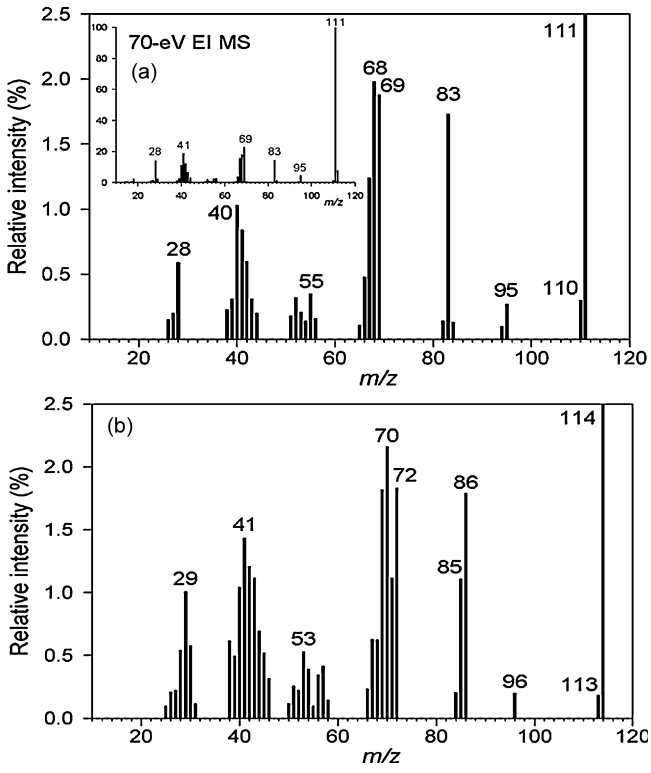

Fig. 6. Collisionally-activated dissociation mass spectrum of [cytosine]•+ obtained as a B/E linked scan. Inset shows the standard 70 eV electron ionization mass spectrum of cytosine [57].

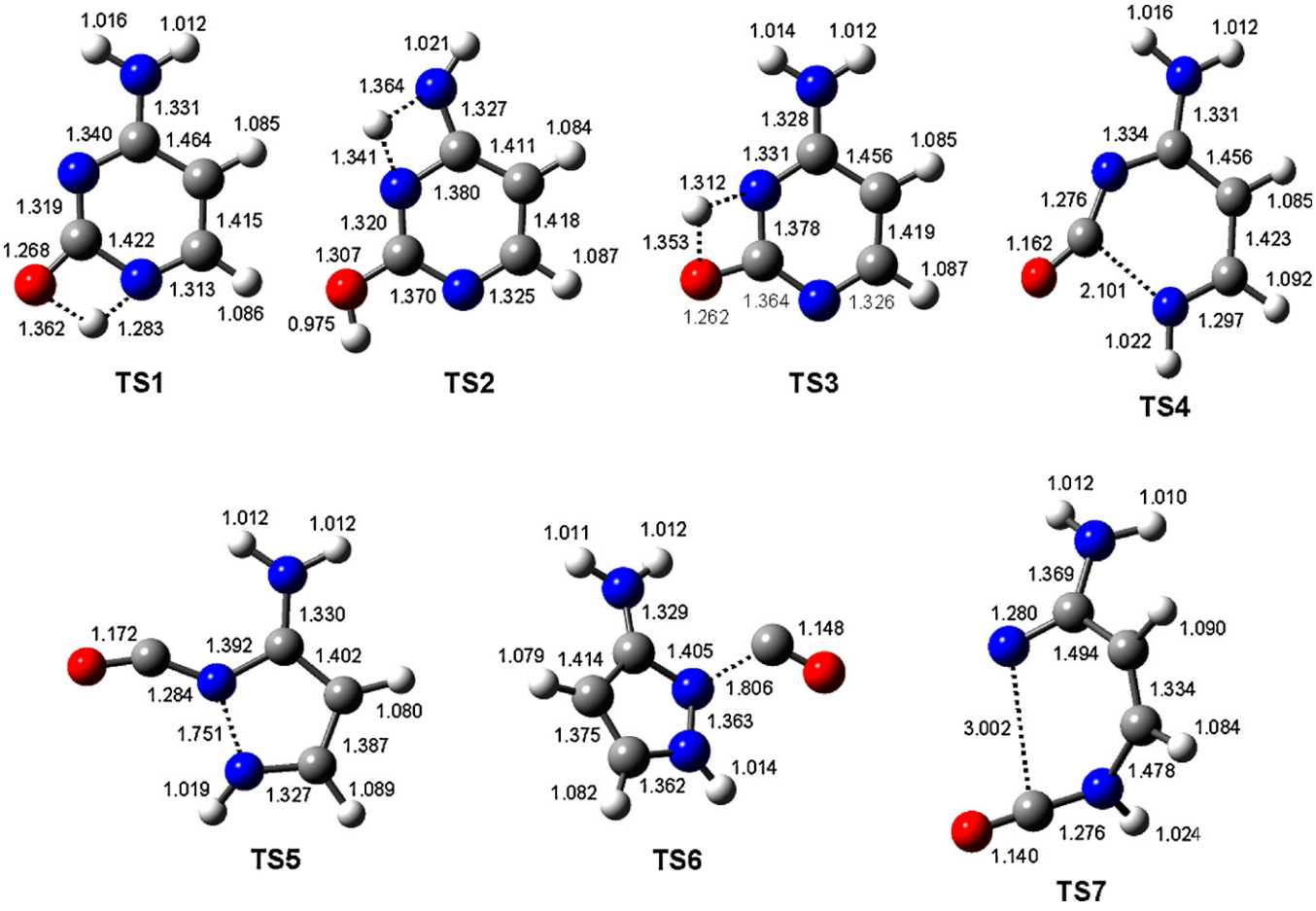

Fig. 7. B3LYP/6-31+G(d,p) optimized structures of transition states for ion isomerizations and dissociation. Bond lengths in angstroms.

The first item to address is the possible interconversion of the low-energy ion tautomers $\mathbf{1}^{\bullet+}$, $\mathbf{2}^{\bullet+}$, $\mathbf{3}^{\bullet+}$, $\mathbf{6}^{\bullet+}$, and $\mathbf{7}^{\bullet+}$. This may proceed by reversible 1,3-proton migrations, e.g., $\mathbf{1}^{\bullet+} \rightarrow \mathbf{2}^{\bullet+} \rightarrow \mathbf{7}^{\bullet+}$ and $\mathbf{3}^{\bullet+} \rightarrow \mathbf{6}^{\bullet+}$, as shown in Scheme 2. As a case in point, we investigated the $\mathbf{1}^{\bullet+} \rightarrow \mathbf{2}^{\bullet+}$ proton migration which was found to proceed through a low-lying transition state (**TS1**) at 134 kJ mol^{-1} above $\mathbf{1}^{\bullet+}$ and 144 kJ mol^{-1} above $\mathbf{2}^{\bullet+}$. The mean internal energy of $\mathbf{1}^{\bullet+}$, when produced in its ground electronic state, is given by the sum of the mean rovibrational enthalpy of **1** at the ion source temperature (37 kJ mol^{-1} at 473 K) and the Franck–Condon energy upon vertical ionization (8 kJ mol^{-1}) and equals $E_{exc} = 37 + 8 = 45$ kJ mol^{-1} [58,59]. This indicates that a major fraction of stable $\mathbf{1}^{\bullet+}$ does not have sufficient energy for unimolecular isomerization to the more stable tautomer $\mathbf{2}^{\bullet+}$. Likewise, the mean internal energy in $\mathbf{2}^{\bullet+}$ by ionization of **2** is $E_{exc} = 35 + 20 = 55$ kJ mol^{-1}, which is insufficient for isomerization to $\mathbf{1}^{\bullet+}$ through **TS1** or to $\mathbf{7}^{\bullet+}$ through **TS2**. Regarding metastable ions $\mathbf{1}^{\bullet+}$ and $\mathbf{2}^{\bullet+}$ with 10^{-5} s lifetimes, RRKM calculations of the isomerization rate constants indicate that most ions with internal energies <160 kJ mol^{-1} will not isomerize on the metastable-ion time scale (Fig. 8). Internal conversion from the first and second (n and π^*) electronically excited states of cytosine cation–radicals, which are produced by electron ionization at ≥1.0 eV above the ground state [4], provides internal energies that are close to or above the isomerization barrier in **TS1**. However, the isomerization is expected to be slow due to the 30–40 kJ mol^{-1} kinetic shifts (Fig. 8a). With more energetic ions, the isomerization kinetics prefers $\mathbf{2}^{\bullet+}$ over $\mathbf{1}^{\bullet+}$, as indicated by the calculated molar fractions for the $\mathbf{2}^{\bullet+} \Leftrightarrow \mathbf{1}^{\bullet+}$ equilibrium. Similar arguments regarding ion interconversion can be used for the $\mathbf{2}^{\bullet+} \rightarrow \mathbf{7}^{\bullet+}$ and $\mathbf{3}^{\bullet+} \rightarrow \mathbf{6}^{\bullet+}$ isomerizations that have somewhat higher barriers for proton migration, e.g., **TS2** at 161 kJ mol^{-1} above $\mathbf{2}^{\bullet+}$, and **TS3** at 155 kJ mol^{-1} above $\mathbf{3}^{\bullet+}$ (Table 3). The energy barriers for isomerizations indicate that it is in principle possible to generate pure isomers $\mathbf{1}^{\bullet+}$, $\mathbf{6}^{\bullet+}$, $\mathbf{7}^{\bullet+}$ and a mixture of rotamers $\mathbf{2}^{\bullet+}$ and $\mathbf{3}^{\bullet+}$, provided that one started from pure neutral tautomers and used a threshold ionization method. However, the mass spectrometric means of distinguishing cytosine cation–radicals are limited, as discussed below.

The elimination of CO is calculated to require a rather low threshold energy (39 kJ mol^{-1}), but involves activation barriers to N–C bond cleavages. Scheme 2 shows the proposed mechanism for the loss of CO from $\mathbf{1}^{\bullet+}$. Dissociation of the N-1–C-2 bond proceeds through a low-lying transition state (**TS4**, $E_{TS4} = 36$ kJ mol^{-1}) to form an open-ring cation–radical $\mathbf{12}^{\bullet+}$ which is only 33 kJ mol^{-1} above $\mathbf{1}^{\bullet+}$. In the next step, the isocyanate group rotates about the N-3–C-4 bond to form a higher-energy isomer $\mathbf{13}^{\bullet+}$ (67 kJ mol^{-1} above $\mathbf{1}^{\bullet+}$) which can cyclize through **TS5** to form a pyrazole ring in the distonic

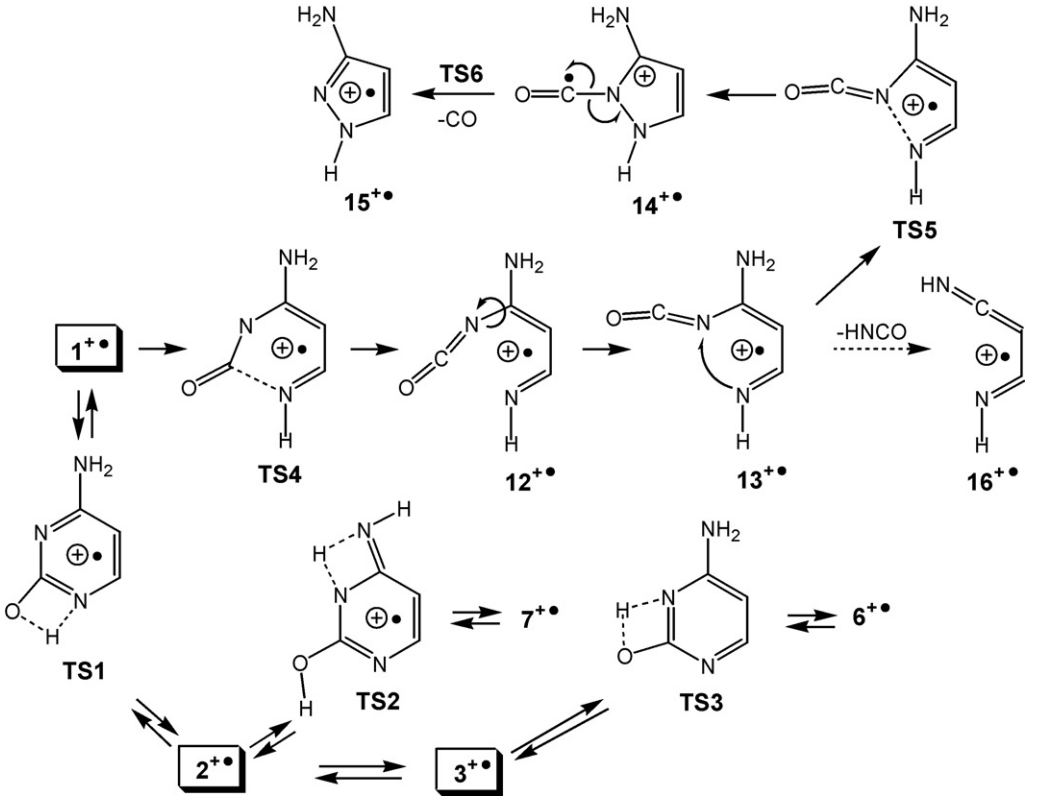

Scheme 2.

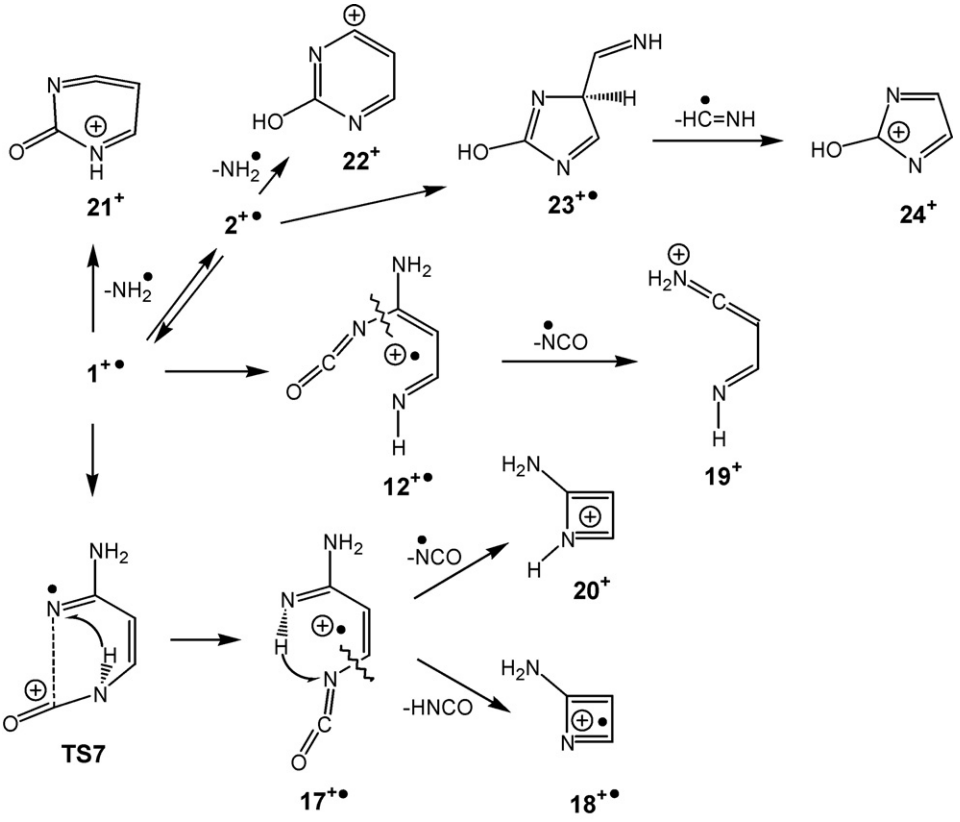

Scheme 3.

intermediate $\mathbf{14}^{\bullet+}$ at 92 kJ mol^{-1} above $\mathbf{1}^{\bullet+}$. Loss of CO from $\mathbf{14}^{\bullet+}$ produces the stable aminopyrazole ion $\mathbf{15}^{\bullet+}$. The potential energy for crossing the highest-energy saddle point **TS5**, which is 169 kJ mol^{-1} above $\mathbf{1}^{\bullet+}$ and 130 kJ mol^{-1} above the products, explains the substantial kinetic energy release in the loss of CO from metastable $\mathbf{1}^{\bullet+}$ ($T_{0.5} = 0.55$ eV = 53 kJ mol^{-1}, Fig. 5). Note that the kinetic energy release is almost exactly equal to the dissociation exothermicity for $\mathbf{14}^{\bullet+} \rightarrow \mathbf{15}^{\bullet+} + CO$ ($\Delta H_{rxn} = -53$ kJ mol^{-1}). However, since $\mathbf{14}^{\bullet+}$ is a local energy minimum and its dissociation to $\mathbf{15}^{\bullet+} + CO$ is exothermic, they are separated by an energy barrier in a transition state for the O=C–N bond cleavage (**TS6**) which was calculated to be 51 kJ mol^{-1} above $\mathbf{14}^{\bullet+}$ (Table 3).

The TS energy in the rate-determining step for loss of CO from $\mathbf{1}^{\bullet+}$ (**TS5**) is $169 - 134 = 35$ kJ mol^{-1} above the energy barrier for $\mathbf{1}^{\bullet+} \rightarrow \mathbf{2}^{\bullet+}$ interconversion (**TS1**). This indicates that $\mathbf{2}^{\bullet+}$ that have sufficient internal energy for dissociation by loss of CO will undergo isomerization to $\mathbf{1}^{\bullet+}$. RRKM calculations of the unimolecular rate constants for $\mathbf{2}^{\bullet+} \rightarrow$ **TS1** $\rightarrow \mathbf{1}^{\bullet+}$ indicate an isomerization with $k = 3 \times 10^4$ s^{-1} in $\mathbf{2}^{\bullet+}$ having an internal energy at the **TS5** dissociation threshold.

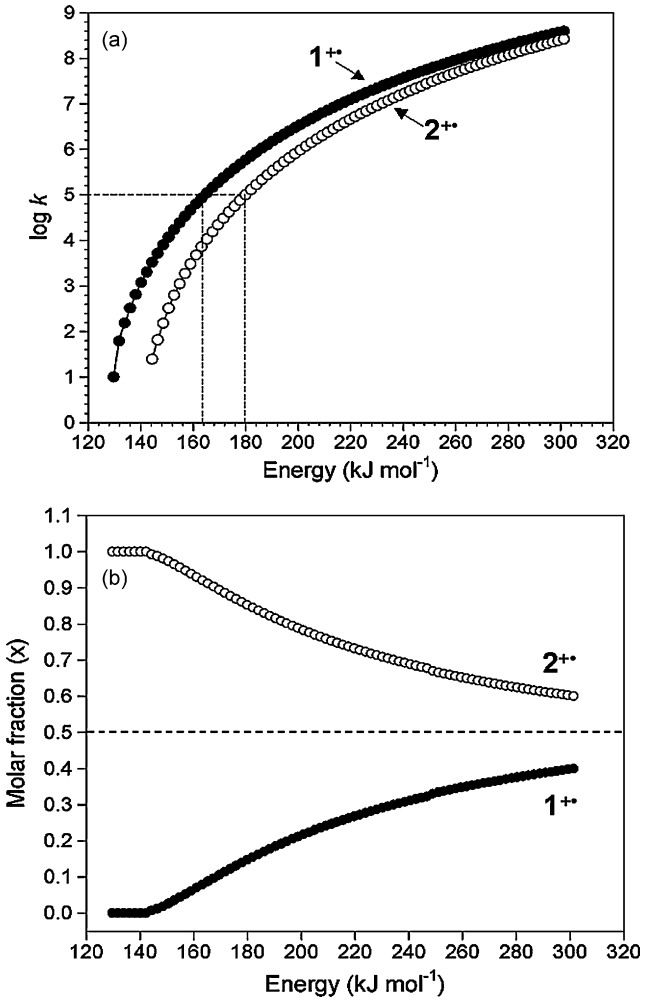

Fig. 8. (a) RRKM unimolecular rate constants for the isomerization $\mathbf{1}^{\bullet+} \rightarrow \mathbf{2}^{\bullet+}$ (full circles) and $\mathbf{2}^{\bullet+} \rightarrow \mathbf{1}^{\bullet+}$ (open circles) isomerizations. (b) Molar fractions of $\mathbf{1}^{\bullet+}$ and $\mathbf{2}^{\bullet+}$ as a function of internal energy.

The elimination of CO competes with the loss of the [CH_2N] radical and an HN=C=O molecule. The latter dissociation may proceed via various mechanisms involving N-1 or N-3. The dissociation involving N-1 may be visualized as starting with a cleavage of the C-2–N-3 bond that requires 223 kJ mol^{-1} in the transition state (**TS7**) and produces an open-ring intermediate $\mathbf{17}^{\bullet+}$ (Scheme 3). Note that this ring opening in $\mathbf{1}^{\bullet+}$ is accompanied by a rotation of the incipient O=C=N-1 group about the N-1–C-6 bond and concomitant proton migration onto N-3. Elimination of HN=C=O from $\mathbf{17}^{\bullet+}$ must involve a reverse proton migration and possibly also a ring closure forming the 2-aminoazacyclobutadiene cation–radical ($\mathbf{18}^{\bullet+}$) at 198 kJ mol^{-1} threshold energy. Alternatively, the elimination of HN=C=O may involve N-3 and proceed via $\mathbf{13}^{\bullet+}$ by proton migration from the NH_2 group to eventually form the 1,3-diiminopropene ion ($\mathbf{16}^{\bullet+}$) at 179 kJ mol^{-1} threshold energy (Scheme 2, Table 3). The fact that the elimination of HN=C=O competes poorly with the loss of CO in the metastable ion spectra is consistent with the higher threshold and transition states energies for the former.

Eliminations of HN=C=O, O=C=N$^{\bullet}$, CO, [C,N,H_2]$^{\bullet}$, and $NH_2^{\bullet}$ are the main primary dissociations of cytosine cation–radicals that are observed in the CAD and EI mass spectra. Loss of O=C=N$^{\bullet}$ can proceed directly from intermediate $\mathbf{12}^{\bullet+}$ by simple cleavage of the N-3–C-4 bond to produce the diazacumulene ion $\mathbf{19}^{+}$ (Scheme 3), or from $\mathbf{17}^{\bullet+}$ with a concurrent ring closure forming protonated 2-aminozacyclobutadiene ($\mathbf{20}^{+}$, Scheme 3). The latter ion is 36 kJ mol^{-1} more stable than $\mathbf{19}^{+}$ (Table 3). The energetically more favorable loss of NCO forming $\mathbf{20}^{+}$ requires 281 kJ mol^{-1} at the thermochemical threshold of the products (Table 3).

Loss of the NH_2 radical from $\mathbf{1}^{\bullet+}$ forming the pyrimid-2(*1H*)-on-4-yl cation ($\mathbf{21}^{+}$, Scheme 3) is another high-energy dissociation that is calculated to require a threshold energy of 341 kJ mol^{-1} (Table 3). A related loss of NH_2 radical from $\mathbf{2}^{\bullet+}$ forming the 2-hydroxypyrimid-4-yl cation ($\mathbf{22}^{+}$) is also substantially endothermic and requires 373 kJ mol^{-1} (Table 3).

Elimination of [C, N, H_2] as HC=NH$^{\bullet}$ or its more stable CH_2=N$^{\bullet}$ isomer is another high-energy dissociation than may involve expulsion of C-4 and N-4 from $\mathbf{2}^{\bullet+}$ through isomerization to intermediate $\mathbf{23}^{\bullet+}$ followed by simple bond cleavage to form the 2-hydroxyimidazol-2-yl cation ($\mathbf{24}^{+}$) at the respective 392 and 359 kJ mol^{-1} threshold energies (Table 3). A simple ring cleavage in $\mathbf{1}^{\bullet+}$ followed by expulsion of a HC=NH radical was calculated to require very high energies at the thermochemical thresholds for the formation of the 4-aminoazet-2-one ($\mathbf{25}^{+}$, Table 3) or oxazol-2-yl ($\mathbf{26}^{+}$, Table 3) cations, which can hardly at all be expected to compete with the loss of CO at internal energies close to the dissociation threshold.

3.5. Neutralization–reionization of cytosine cation–radicals

Collisional electron transfer to [cytosine]$^{\bullet+}$ cation–radicals results in the formation of stable neutral molecules that are detected as intense survivor ions in the $^{+}NR^{+}$ mass spec-

tra. The spectra obtained by collisional neutralization with trimethylamine (IE_v = 8.44–8.56 eV) [57] and dimethyldisulfide (IE_v = 8.96 eV) [57] on different instruments are remarkably similar (cf. Figs. 5c and 9a). Compared with the vertical ionization and recombination energies of **1**–**4** (Table 2), the collisional electron transfer from trimethylamine and dimethyldisulfide is only slightly exothermic and endothermic, respectively. Such small differences in ionization and recombination energies usually do not affect $^{+}NR^{+}$ mass spectra [60].

The dissociations observed upon $^{+}NR^{+}$ produced the same type of fragments as those in CAD. This overall similarity indicates that the cytosine molecules formed by collisional electron transfer did not dissociate extensively, and most of the fragmentations observed occurred following collisional reionization. In line with this, the differences that are seen in the fragment relative intensities, e.g., smaller fragments (*m/z* 28, 40, 41) being relatively more intense in $^{+}NR^{+}$, while *m/z* 95 and 83 being less intense, may be assigned to consecutive dissociations following collisional reionization [61]. The *m/z* 28 fragment, presumably $CO^{\bullet+}$, may originate from reionization of neutral CO formed by collateral dissociation of $[cytosine]^{\bullet+}$ in the neutralizing collision [62]. Collisional activation of neutral [cytosine] produced by electron transfer resulted in increased intensities of the low-mass fragments in the $^{+}NCR^{+}$ mass spectrum (Fig. 9b). However, this collisional activation did not open new channels that could be assigned to neutral dissociations. We conclude that the $^{+}NR^{+}$ mass spectra reflect mainly ion dissociations that are promoted by sequential excitation by the neutralizing and reionizing collisions.

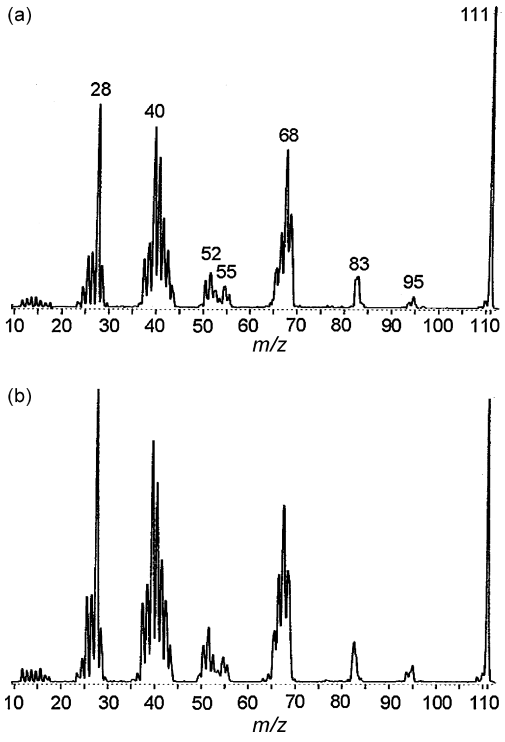

Fig. 9. (a) Neutralization (CH_3SSCH_3)/reionization (O_2) mass spectrum of $[cytosine]^{\bullet+}$. (b) Neutralization (CH_3SSCH_3)/neutral collisional activation (He)/reionization (O_2) mass spectrum of $[cytosine]^{\bullet+}$.

4. Conclusions

Cytosine molecules and cation–radicals represent complex systems of several tautomers of similar stabilities within each group. Gas-phase cytosine exists as four major tautomers at thermal equilibrium. Ionization by electron-impact is predicted to form a mixture of cytosine cation–radicals. Interconversion of ion tautomers by intramolecular hydrogen migrations requires activation energies that are in general lower than those for lowest-energy dissociation by loss of CO. Thus, six low-energy cation–radical tautomers can equilibrate before dissociation. Collisional neutralization of cytosine cation–radical by femtosecond electron transfer produces stable molecules that do not undergo substantial dissociation.

Acknowledgements

F.T. thanks the National Science Foundation for support through grants CHE-0349595 for experiments and CHE-0342956 for computations. The Computational Chemistry Center at the UW Department of Chemistry receives joint support by the NSF and University of Washington. C.W. thanks the NSF (CHE-0111128) for generous financial support. Thanks are due to Dr. Martin Sadilek for technical assistance with mass spectra measurements. The Jeol HX-110 mass spectrometer was a generous donation from the former Seattle Biomembrane Institute by courtesy of Professor S. Hakomori.

References

[1] C. Von Sonntag, in: W.A. Glass, M.N. Varma (Eds.), Physical and Chemical Mechanisms in Molecular Radiation Biology, Plenum Press, New York, 1991, p. 287.
[2] N.S. Hush, A.S. Cheung, Chem. Phys. Lett. 34 (1975) 11.
[3] V.M. Orlov, A.N. Smirnov, Ya.M. Varshavsky, Tetrahedron Lett. (1976) 4377.
[4] C. Yu, S. Peng, I. Akiyama, J. Lin, P.R. LeBreton, J. Am. Chem. Soc. 100 (1978) 2303.
[5] J. Lin, C. Yu, S. Peng, I. Akiyama, K. Li, L.K. Lee, P.R. LeBreton, J. Am. Chem. Soc. 102 (1980) 4627.
[6] C. Yu, T.J. O'Donnell, P.R. LeBreton, J. Phys. Chem. 85 (1981) 3851.
[7] M.D. Sevilla, B. Besler, A.-O. Colson, J. Phys. Chem. 99 (1995) 1060.
[8] R. Improta, G. Scalmani, V. Barone, Int. J. Mass Spectrom. 201 (2000) 321.
[9] S.D. Wetmore, R.J. Boyd, L.A. Eriksson, Chem. Phys. Lett. 322 (2000) 129.
[10] S. Steenken, Chem. Rev. 89 (1989) 503.
[11] D.M. Close, E. Sagstuen, W.H. Nelson, J. Chem. Phys. 82 (1985) 4386.
[12] E. Sagstuen, E.O. Hole, W.H. Nelson, D.M. Close, J. Phys. Chem. 96 (1992) 8269.
[13] S.D. Wetmore, F. Himo, R.J. Boyd, L.A. Eriksson, J. Phys. Chem. B (1998) 7484.
[14] J. Llano, L.A. Eriksson, Phys. Chem. Chem. Phys. 6 (2004) 2426.
[15] (a) J.A. McCloskey, in: J.A. McCloskey (Ed.), Methods in Enzymology, vol. 198, Academic Press, San Diego, 1990, p. 771;
(b) A.S. Plaziak, Wiadom. Chem. 47 (1993) 51;
(c) R. Tembreull, D.M. Lubman, Anal. Chem. 58 (1986) 1299;
(d) G.B. Mohamed, A. Nazareth, M.J. Hayes, R.W. Giese, P. Vouros, J. Chromatogr. 314 (1984) 211;
(e) J.M. Rice, G.O. Dudek, M. Barber, J. Am. Chem. Soc. 87 (1965) 4569.
[16] F. Tureček, J.K. Wolken, J. Phys. Chem. A 105 (2001) 8740.

[17] X. Chen, E.A. Syrstad, P. Gerbaux, M.T. Nguyen, F. Tureček, J. Phys. Chem. A 108 (2004) 9283.
[18] F. Tureček, Adv. Quant. Chem. 52 (2007) 89.
[19] J. Sponer, P. Hobza, Collect. Czech. Chem. Commun. 68 (2003) 2231.
[20] P.M. Curtis, B.W. Williams, R.F. Porter, Chem. Phys. Lett. 65 (1979) 296.
[21] P.C. Burgers, J.L. Holmes, A.A. Mommers, J.K. Terlouw, Chem. Phys. Lett. 102 (1983) 1.
[22] P.O. Danis, C. Wesdemiotis, F.W. McLafferty, J. Am. Chem. Soc. 105 (1983) 7454.
[23] (a) For recent reviews see: F. Turecek, Top. Curr. Chem. 225 (2003) 77;
(b) D.V. Zagorevskii, in: J.A. McCleverty, T.J. Meyer (Eds.), Comprehensive Coordination Chemistry II, Elsevier, Oxford, 2004, p. 381;
(c) F. Tureček, in: P.B. Armentrout (Ed.), Encyclopedia of Mass Spectrometry, vol. 1, Elsevier, Amsterdam, 2003, p. 528 (Chapter 7);
(d) D.V. Zagorevskii, Coord. Chem. Rev. 225 (2002) 5;
(e) P. Gerbaux, C. Wentrup, R. Flammang, Mass Spectrom. Rev. 19 (2000) 367;
(f) D.V. Zagorevskii, J.L. Holmes, Mass Spectrom. Rev. 18 (1999) 87;
(g) C. Schalley, G. Hornung, D. Schröder, H. Schwarz, Chem. Soc. Rev. 27 (1998) 91.
[24] M.J. Polce, M.M. Cordero, C. Wesdemiotis, P.A. Bott, Int. J. Mass Spectrom. Ion Process. 113 (1992) 35.
[25] F. Tureček, M. Gu, S.A. Shaffer, J. Am. Soc. Mass Spectrom. 3 (1992) 493.
[26] F. Tureček, Org. Mass Spectrom. 27 (1992) 1087.
[27] M.J. Frisch, et al., Gaussian 03, Revision B.05, Gaussian Inc., Pittsburgh, PA, 2003.
[28] A.D. Becke, J. Chem. Phys. 98 (1993) 1372.
[29] A.D. Becke, J. Chem. Phys. 98 (1993) 5648.
[30] P.J. Stephens, F.J. Devlin, C.F. Chabalowski, M.J. Frisch, J. Phys. Chem. 98 (1994) 11623.
[31] C. Møller, M.S. Plesset, Phys. Rev. 46 (1934) 618.
[32] F. Tureček, C.J. Cramer, J. Am. Chem. Soc. 117 (1995) 12243.
[33] F. Tureček, J. Phys. Chem. A 102 (1998) 4703.
[34] (a) F. Tureček, M. Polášek, A.J. Frank, M. Sadílek, J. Am. Chem. Soc. 122 (2000) 2361;
(b) M. Polášek, F. Tureček, J. Am. Chem. Soc. 122 (2000) 9511;
(c) F. Tureček, C. Yao, J. Phys. Chem. A 107 (2003) 9221;
(d) P.R. Rablen, J. Am. Chem. Soc. 122 (2000) 357;
(e) P.R. Rablen, J. Org. Chem. 65 (2000) 7930;
(f) P.R. Rablen, K.H. Bentrup, J. Am. Chem. Soc. 125 (2003) 2142;
(g) M. Hirama, T. Tokosumi, T. Ishida, J. Aihara, Chem. Phys. 305 (2004) 307;
(h) Y.M.E. Fung, H. Liu, T.W.D. Chan, J. Am. Soc. Mass Spectrom. 17 (2006) 757.
[35] J. Čížek, J. Paldus, L. Šroubková, Int. J. Quant. Chem. 3 (1969) 149.
[36] G.D. Purvis, R.J. Bartlett, J. Chem. Phys. 76 (1982) 1910.
[37] T.H. Dunning Jr., J. Chem. Phys. 90 (1989) 1007.
[38] L. Zhu, W.L. Hase, Quantum Chemistry Program Exchange, Indiana University, Bloomington, 1994, Program No. QCPE 644.
[39] A.J. Frank, M. Sadílek, J.G. Ferrier, F. Tureček, J. Am. Chem. Soc. 119 (1997) 12343.
[40] R.J. McClure, B.M. Craven, Acta Cryst. B29 (1973) 1234.
[41] H.P. Weber, B.M. Craven, R.K. McMullan, Acta Cryst. B36 (1980) 645.
[42] M. Szczesniak, K. Szczepaniak, J.S. Kwiatkowski, K. Kubulat, W.B. Person, J. Am. Chem. Soc. 110 (1988) 8319.
[43] I.R. Gould, V.S. Darren, P. Young, I.H. Hillier, J. Org. Chem. 57 (1992) 4434.
[44] A. Destexhe, J. Smets, L. Adamowicz, G. Maes, J. Phys. Chem. 98 (1994) 1506.
[45] R.J. Hall, N.A. Burton, I.H. Hiller, P.E. Young, Chem. Phys. Lett. 220 (1994) 129.
[46] L. Paglieri, G. Corongiu, D.A. Estrin, Int. J. Quantum Chem. 56 (1995) 615.
[47] L. Gorb, J. Leszczynski, Int. J. Quant. Chem. 70 (1998) 855.
[48] S. Morpurgo, M. Bossa, G.O. Morpurgo, Adv. Quant. Chem. 36 (1999) 169.
[49] J.R. Sambrano, A.R. de Souza, J.J. Queralt, J. Andres, Chem. Phys. Lett. 317 (2000) 437.
[50] G. Fogarasi, P.G. Szalay, Chem. Phys. Lett. 356 (2002) 383.
[51] R. Kobayashi, J. Phys. Chem. A 102 (1998) 10813.
[52] S.A. Trygubenko, T.V. Bogdan, M. Rueda, M. Orozco, F.J. Luque, J. Šponer, P. Slavíček, P. Hobza, Phys. Chem. Chem. Phys. 4 (2002) 4192.
[53] Y. Apeloig, in: Z. Rappoport (Ed.), The Chemistry of Enols, Wiley, Chichester, 1990, p. 2 (Chapter 1).
[54] F. Tureček, in: Z. Rappoport (Ed.), The Chemistry of Enols, Wiley, Chichester, 1990, p. 95 (Chapter 3).
[55] F. Tureček, L. Brabec, J. Korvola, J. Am. Chem. Soc. 110 (1988) 7984.
[56] W.L. Fitch, A.D. Sauter, Anal. Chem. 55 (1983) 832.
[57] NIST Standard Reference Database No. 69, June 2005 release. http://webbook.nist.gov.
[58] J.K. Wolken, F. Tureček, J. Am. Chem. Soc. 121 (1999) 6010.
[59] F. Tureček, Int. J. Mass Spectrom. 227 (2003) 327.
[60] V.Q. Nguyen, F. Tureček, J. Mass Spectrom. 31 (1996) 843.
[61] S. Beranova, C. Wesdemiotis, J. Am. Soc. Mass Spectrom. 5 (1994) 1093.
[62] M.J. Polce, S. Beranova, M.J. Nold, C. Wesdemiotis, J. Mass Spectrom. 31 (1996) 1073.